

Magnetic Order of the Hexagonal Rare Earth Manganite $\text{Dy}_{0.5}\text{Y}_{0.5}\text{MnO}_3$

Joel S. Helton^{1,*}, Deepak K. Singh^{1,2}, Harikrishnan S. Nair^{3,4}, and Suja Elizabeth³

¹*NIST Center for Neutron Research, National Institute of Standards and Technology, Gaithersburg, MD 20899, USA*

²*Department of Materials Science and Engineering,*

University of Maryland, College Park, MD 20742, USA

³*Department of Physics, Indian Institute of Science, Bangalore 560012, India and*

⁴*Institut für Festkörperforschung, Forschungszentrum Jülich, D-52425 Jülich, Germany*

(Dated: October 11, 2024)

Hexagonal $\text{Dy}_{0.5}\text{Y}_{0.5}\text{MnO}_3$, a multiferroic rare earth manganite with geometrically frustrated antiferromagnetism, has been investigated with neutron diffraction measurements. Below 3.4 K magnetic order is observed on both the Mn (antiferromagnetic) and Dy (ferrimagnetic) sublattices that is identical to that of undiluted hexagonal (h) DyMnO_3 . The Mn moments undergo a spin reorientation transition between 3.4 K and 10 K, with antiferromagnetic order of the Mn sublattice persisting up to 70 K; the antiferromagnetic order in this intermediate temperature phase is distinct from that observed in undiluted (h) DyMnO_3 or other (h) RMnO_3 materials with a magnetic R ion, yielding a qualitatively new phase diagram not seen in other hexagonal rare earth manganites. A magnetic field applied parallel to the crystallographic c -axis will drive a transition from the intermediate temperature antiferromagnetic phase into the low temperature ferrimagnetic phase with relatively little hysteresis.

PACS numbers: 75.25.-j, 75.85.+t, 75.50.Ee, 75.47.Lx

I. INTRODUCTION

The crystalline structure of rare earth manganites (RMnO_3 with $R = \text{Y, Sc, or a lanthanide}$) is determined by the ionic radius of the R^{3+} cation. Materials with a large R^{3+} ionic radius ($R = \text{La through Tb}$) crystallize in an orthorhombic perovskite structure, while materials with a smaller R^{3+} ionic radius ($R = \text{Y, Sc, or Ho through Lu}$)¹⁻⁶ crystallize in a hexagonal structure. DyMnO_3 typically crystallizes in the orthorhombic structure,⁷ but with proper growth conditions hexagonal (h) DyMnO_3 can be stabilized.^{8,9} The hexagonal rare earth manganites, (h) RMnO_3 , are paraelectric at very high temperatures but display a structural transition ($T_C \approx 1000$ K) to a ferroelectric phase with the noncentrosymmetric $P6_3cm$ space group.¹⁰ The (h) RMnO_3 materials feature slightly distorted triangular lattice planes of Mn ions; the antiferromagnetic nearest-neighbor exchange interaction leads to geometrically frustrated magnetism. Below a Néel temperature of ≈ 100 K these materials are multiferroic, with easy-plane antiferromagnetic order of the Mn sublattice coexisting with the ferroelectric order. Many hexagonal rare earth manganites display one or more spin reorientation transitions of the Mn moments at lower temperatures;¹¹ the R ions also form distorted triangular lattice planes and, for magnetic ions, will order along the c -axis. Several of these materials have attracted interest because of significant magnetoelectric^{12,13} or magnetoelastic¹⁴ effects. Despite the structural similarities between the various members of the (h) RMnO_3 family, the magnetically ordered structures are often different with structures that order according to each of the four one-dimensional irreducible representations of the point group observed in at least one material. The dependence of the magnetic ordering

of the Mn sublattice on the rare earth element has been attributed to the ionic radius of the R^{3+} cation¹⁵ or a biquadratic $3d-4f$ magnetic coupling.¹⁶

Hexagonal (h) DyMnO_3 , with the largest rare earth ionic radius of this series, features an interesting magnetic phase diagram.^{9,16,17} In the low temperature phase (below ≈ 8 K) both the Mn and Dy sublattices are magnetically ordered according to the Γ_2 irreducible representation. At a temperature around 8 K the Mn moments undergo a spin reorientation transition, and are ordered in the Γ_4 representation up to 68 K.¹⁶ X-ray resonant magnetic scattering measurements also find a weak Dy moment in this temperature range, ordering according to the Γ_3 representation.¹⁷ This incompatible order, with different irreducible representations present on the two sublattices, calls into question long standing assumptions about the rigidity of the $3d-4f$ interaction in (h) RMnO_3 materials.¹⁶ We report single crystal neutron diffraction studies of hexagonal $\text{Dy}_{0.5}\text{Y}_{0.5}\text{MnO}_3$ (DYMO). Doping the rare earth site with nonmagnetic Y^{3+} ions allows investigation of the effects of magnetic dilution and rare earth site disorder on the magnetically ordered structures of the material. We find that the low temperature magnetic phase is ordered in the ferrimagnetic Γ_2 representation, identical to that observed in undiluted (h) DyMnO_3 . However, the magnetic order of the Mn moments in the intermediate temperature antiferromagnetic phase is either the Γ_1 or Γ_3 representation. With either of these magnetic structures, the spin reorientation transition from the low temperature Γ_2 phase into the intermediate temperature phase will be different from the zero field reorientation transitions observed in other hexagonal rare earth manganites.

II. EXPERIMENT

Large, high quality single crystal samples of $\text{Dy}_{0.5}\text{Y}_{0.5}\text{MnO}_3$ were prepared as previously reported.¹⁸ DYMO crystallizes in the hexagonal $P6_3cm$ space group (#185) with lattice parameters (at 300 K) of $a = b = 6.161(1)$ Å and $c = 11.446(2)$ Å. As in other hexagonal rare earth manganites, Mn^{3+} ions ($S = 2$) occupy the $6c$ positions at $(x, 0, 0)$ with $x \approx \frac{1}{3}$ and equivalent positions. A material with $x = \frac{1}{3}$ would feature perfect triangular lattice planes; in DYMO $x = 0.3379(4)$ yielding a slightly distorted triangular lattice. The rare earth R^{3+} ions occupy two crystallographically distinct sites, at the $2a$ and $4b$ Wyckoff positions. These rare earth ions also form distorted triangular lattice planes; in our sample the rare earth sites are occupied with equal probability by nonmagnetic Y^{3+} ions and ${}^6H_{15/2}$ Dy^{3+} ions ($gJ = 10 \mu_B$). Previously reported specific heat measurements¹⁸ found peaks at 3 K and 68 K; in analogy with other hexagonal rare earth manganites such as DyMnO_3 it was suggested that these peaks correspond to the onset of antiferromagnetic order of the Mn lattice, $T_N^{\text{Mn}} \approx 68$ K, and ferrimagnetic order of Dy moments on the rare earth lattice, $T_N^{\text{Dy}} \approx 3$ K.

Neutron diffraction experiments were carried out using the BT9 thermal triple-axis spectrometer at the NIST Center for Neutron Research. The neutron initial and final energies were selected using the $(2\ 0\ 0)$ reflection of the pyrolytic graphite (PG) monochromator and analyzer. We used $40'-47'-40'$ -Open collimation as well as two PG filters to reduce contamination of the beam with higher-order neutron wavelengths. The detailed temperature dependence of four magnetic reflections (shown in Fig. 1) was measured using a large (≈ 1 g) single crystal mounted in the $(H\ 0\ L)$ scattering plane and a fixed neutron energy of 30.5 meV ($\lambda = 1.64$ Å). Determination of the magnetic structure and refinement of the ordered moments utilized diffraction measurements taken at 41 reflections at temperatures of 1.6 K, 25 K, and 120 K at a fixed neutron energy of 30.5 meV. In order to minimize absorption of neutrons by the sample, these measurements were taken with small single crystals: an 8 mg sample mounted in the $(H\ 0\ L)$ scattering plane and a 6 mg sample mounted in the $(H\ K\ 0)$ scattering plane. The intensity of the $(1\ 0\ 0)$ and $(3\ \bar{1}\ 0)$ reflections in a magnetic field (shown in Figs. 3 and 4) were measured on the 6 mg sample mounted in the $(H\ K\ 0)$ scattering plane; the sample was placed inside a helium flow dewar with a minimum temperature of 4 K inserted into a 7 Tesla vertical field superconducting magnet. These data were taken at a fixed neutron energy of 14.7 meV ($\lambda = 2.36$ Å). All neutron diffraction data are reported in terms of the integrated intensity, integrated over a rocking curve (θ scan) through the peak position.

The allowed magnetic structures in DYMO correspond to the six irreducible representations of the $P6_3cm$ space group with propagation vector $\vec{k} = 0$; as in other hexago-

nal rare earth manganites, only the four one-dimensional irreducible representations are required to describe the observed structures.^{19,20} Of the four one-dimensional representations, the Γ_1 and Γ_3 representations are almost perfectly homometric with each other so that differentiating between them with neutron scattering is exceptionally difficult; the Γ_2 and Γ_4 representations are likewise almost perfectly homometric with one another. Unambiguous differentiation between these magnetic structures often requires complementary measurement techniques such as optical second harmonic spectroscopy.^{1,21} Yet, when combined with other knowledge such as the bulk magnetization or the nature of spin reorientation transitions, neutron scattering can still be a useful technique in analyzing the magnetic structures of hexagonal rare earth manganites.

III. RESULTS

Figure 1 displays the temperature dependence of the integrated intensities of the $(1\ 0\ 0)$, $(1\ 0\ 1)$, $(2\ 0\ 0)$, and $(2\ 0\ 1)$ magnetic Bragg reflections measured while warming from 2.1 K to 130 K. The high temperature structural contributions to the intensities have been subtracted. At 2.1 K all four reflections display magnetic intensity, with the $(1\ 0\ 1)$ reflection the strongest. Between 2.1 K and 3.4 K the measured intensities of the $(H\ 0\ 1)$ reflections remain constant while the intensities of the $(H\ 0\ 0)$ reflections steadily decrease with increasing temperature, with an intensity at 3.4 K that is about 68% that of the base temperature intensity. Upon increasing the temperature beyond 3.4 K, the intensities of the $(H\ 0\ 0)$ peaks steadily increase while the intensities of the $(H\ 0\ 1)$ peaks decrease so that the $(1\ 0\ 0)$ reflection becomes the strongest measured; this rapid change in intensity persists only to around 10 K. This will be shown to correspond to a spin reorientation transition of the Mn moments, and also explains the 10 K anomaly reported¹⁸ in the derivative of $1/\chi$. Above 10 K the intensity of all peaks slowly decrease until reaching zero at 70 K. The intensity can be fit to an order parameter form: $I(T) \propto (|T - T_N|/T_N)^{2\beta}$; the dotted red line in Fig. 1 is a fit of the $(1\ 0\ 0)$ intensity to this form with $\beta = 0.25 \pm 0.05$.

A. Zero Field Magnetic Order

A set of magnetic reflections was measured at 1.6 K and used to determine the low temperature magnetic structure of DYMO; any structural contributions to the reflections were removed by subtracting the 120 K intensity. We find that the Γ_2 irreducible representation (magnetic space group $P6_3c'm'$) and the Γ_4 irreducible representation ($P6_3c'm$) fit the data equally well. Other irreducible representations as well as orderings with different magnetic space groups for the Mn and Dy mo-

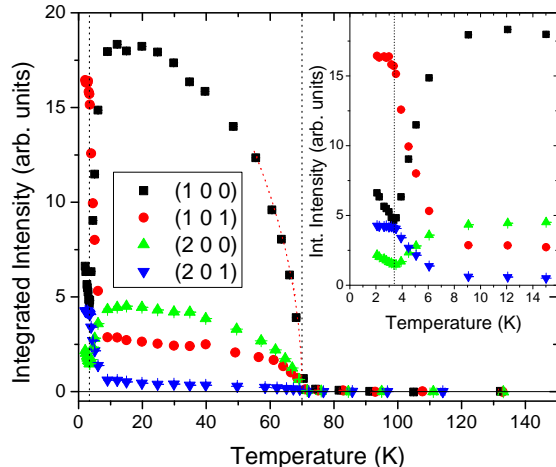


FIG. 1: (color online) Integrated intensities of the (1 0 0), (1 0 1), (2 0 0), and (2 0 1) magnetic Bragg reflections as a function of temperature. All data were measured while warming. The inset shows a closer view of the low temperature portion of the graph. Transitions are observed at $T_N^{\text{Mn}} = 70$ K and $T_N^{\text{Dy}} = 3.4$ K; these temperatures are designated with dashed vertical lines. The red dotted line reflects a fit of the (1 0 0) intensity to an order parameter form with $\beta = 0.25 \pm 0.05$. Error bars throughout this article are statistical in nature and represent one standard deviation.

ments are inconsistent with the data. The Γ_4 representation is antiferromagnetic while the Γ_2 representation is ferrimagnetic. DYMO is ferrimagnetic below T_N^{Dy} ; therefore the low temperature magnetic structure of DYMO can be confirmed as the Γ_2 irreducible representation as shown in Fig. 2(a). Undoped hexagonal DyMnO_3 is also ferrimagnetic in the low temperature phase and has likewise been found to order with this structure.¹⁷ The Dy moments on the rare earth sites are ferrimagnetically ordered along the c -axis, with moments on the $2a$ and $4b$ sites antiparallel to each other. The Mn ions are ordered in a 120° antiferromagnetic arrangement, with all Mn moments around a triangle centered at $(0, 0, z)$ pointing towards the center of the triangle. A refinement of the magnetic reflections reveals ordered moments of $3.7 \pm 0.4 \mu_B$ for the Mn ions and $3.1 \pm 0.3 \mu_B$ for the Dy ions. The Mn ordered moment is close to the full moment value, but the Dy ordered moment is considerably reduced from the full $10 \mu_B$ value of the ${}^6\text{H}_{15/2}$ Dy^{3+} ions suggesting strong fluctuations of the Dy moments in the ordered phase. When magnetic domains are aligned this will lead to a net magnetization of $3.1 \pm 0.3 \mu_B$ per unit cell (or $0.52 \pm 0.05 \mu_B$ per formula unit), which is consistent with the reported bulk spontaneous magnetization at 2 K.¹⁸ Allowing for different ordered moments on the Dy $4b$ and $2a$ sites did not appreciably improve the fit, nor could allowing for different moments on these sites produce a comparably good fit while yielding a net moment consistent with magnetization measurements.

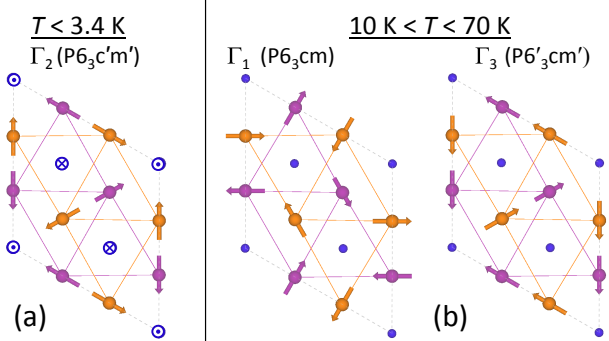


FIG. 2: (color online) (a) Magnetic structure in the low temperature phase, as determined at $T = 1.6$ K. The structure belongs to the $P6_3c'm'$ magnetic space group (Γ_2 irreducible representation). Mn ions at $z = 0$ are shown in purple, Mn ions at $z = 1/2$ are shown in orange, and the rare earth ions are shown in blue. The refined ordered moments are $3.7 \pm 0.4 \mu_B$ on the Mn ions and $3.1 \pm 0.3 \mu_B$ on the Dy ions. (b) The two possible magnetic structures for the intermediate temperature range, determined at $T = 25$ K: $P6_3cm$ magnetic space group (Γ_1 irreducible representation) on the left and $P6'_3cm'$ magnetic space group (Γ_3) on the right. The Mn ordered moment is $3.5 \pm 0.4 \mu_B$, while the Dy lattice is effectively paramagnetic. The Γ_1 structure can transform into the Γ_2 structure through a spin reorientation transition where all Mn moments rotate 90° counterclockwise, while a transformation from Γ_3 to Γ_2 would require a 180° rotation of only one layer of Mn moments.

It was previously noted that, in the data displayed in Fig. 1, the intensities of the (1 0 1) and (2 0 1) magnetic peaks are temperature independent while the intensities of the (1 0 0) and (2 0 0) peaks decrease continuously with increasing temperature in the low temperature phase below 3.4 K. When ordering in the Γ_2 representation, the magnetic intensities of the $(H 0 1)$ reflections are independent of the ordered moment of the Dy ions and depend only on the moment of the Mn ions while the magnetic intensities of the $(H 0 0)$ reflections are independent of the ordered moment of the Mn ions and depend only on the moment of the Dy ions. In particular, the magnetic structure factors of the (1 0 0) and (1 0 1) Bragg reflections can be written as

$$|F_M(\vec{Q}_{100})| = \left\{ \left| \frac{\gamma r_0}{2} \right| f_{\text{Dy}}(Q_{100}) \right\} 2\mu_{\text{Dy}}$$

$$|F_M(\vec{Q}_{101})| = \left\{ \left| \frac{\gamma r_0}{2} \right| f_{\text{Mn}}(Q_{101}) \right\} 4\sin^2(\pi x) \mu_{\text{Mn}} \quad (1)$$

where γ is the neutron gyromagnetic ratio, r_0 is the classical electron radius ($|\frac{\gamma r_0}{2}| = 2.695$ fm), $f_{\text{Dy}}(Q)$ and $f_{\text{Mn}}(Q)$ are the Dy and Mn magnetic form factors, μ_{Dy} and μ_{Mn} are the sizes of the Dy and Mn ordered moments, and $x \approx 1/3$ describes the position of the Mn ions within the unit cell. Thus we can conclude that the ordered moment of the Mn ions is constant in this tem-

perature range, while the ordered moment of the Dy ions decreases continuously with increasing temperature.

The magnetic structure in the intermediate temperature range ($10 \text{ K} < T < 70 \text{ K}$) was determined using a set of reflections measured at 25 K; any structural contributions to the reflections were again removed by subtracting the intensity measured at 120 K. The magnetic structure in this temperature range can be explained by assuming an ordered moment on only the Mn lattice. Element specific x-ray resonant magnetic scattering measurements on hexagonal DyMnO_3 ¹⁷ and HoMnO_3 ²² have reported a weak rare earth moment at comparable temperatures; while DYMO might similarly feature a weak Dy ordered moment in this intermediate temperature range, neutron scattering measurements will be sensitive to only the much larger ordered moment of the Mn sublattice. We find that two of the allowed magnetic structures, the Γ_1 irreducible representation (magnetic space group $P6_3cm$) and the Γ_3 representation ($P6'_3cm'$), fit the data roughly equally well with a refined Mn ordered moment of $3.5 \pm 0.4 \mu_B$. These magnetic structures are shown in Fig. 2(b). It should be noted that neither of these possibilities are consistent with the intermediate temperature structure of the Mn moments in (h) DyMnO_3 , which order in Γ_4 ($P6_3c'm$).¹⁶ The ordered moment of the Mn ions at 25 K is comparable in size to that determined at 1.6 K, suggesting a spin reorientation transition where Mn spins rotate between 3.4 K and 10 K with little change in magnitude.

Although these neutron diffraction experiments can not directly differentiate between the Γ_1 and Γ_3 representations, we can draw some distinctions between the two by considering the nature of spin reorientation transitions in hexagonal rare earth manganites. A magnetic structure in the Γ_1 irreducible representation can be transformed into the Γ_2 representation through a 90° counterclockwise rotation of all Mn moments. Meanwhile, a transformation of a structure in the Γ_3 representation as shown in Fig. 2(b) into the Γ_2 representation would require a 180° rotation of only the Mn moments in the $z = \frac{1}{2}$ plane. In other hexagonal rare earth manganites, it has been suggested²³ that spin reorientation transitions between the four irreducible representations occur via in-phase or anti-phase rotations where the moments in adjacent Mn layers rotate with an equal (in-phase) or opposite (anti-phase) direction. For example, the Mn moments in HoMnO_3 display an in-phase reorientation transition¹¹ (Γ_4 to Γ_3) at $T \approx 40 \text{ K}$ and an anti-phase transition (Γ_3 to Γ_1) at $T \approx 8 \text{ K}$, while the Mn moments in (h) DyMnO_3 display an anti-phase rotation¹⁶ (Γ_4 to Γ_2) at $T \approx 8 \text{ K}$. Further, while materials such as ScMnO_3 ,² $\text{Er}_x\text{Y}_{1-x}\text{MnO}_3$,²⁴ and YMnO_3 under pressure¹⁵ have been reported to feature broad temperature ranges where the magnetic structure is not one of the four irreducible representations, the observed structures can still be described as an in-phase or anti-phase rotation of all Mn moments away from one of the principal structures. The intermediate structures encountered

during an in-phase rotation display a reduced symmetry of either $P6_3$ or $P6'_3$, while those encountered during an anti-phase rotation have $P3c$ or $P3c'$ symmetry. Thus, while both the Γ_1 and Γ_3 magnetic structures are consistent with the neutron diffraction data obtained in the intermediate temperature range ($10 \text{ K} < T < 70 \text{ K}$), only the Γ_1 structure would be consistent with the spin reorientation transitions observed in other hexagonal rare earth manganites.

B. Field Dependence

Below $T_N^{\text{Dy}} \approx 3 \text{ K}$, DYMO is ferrimagnetic; isothermal magnetization measurements with $\vec{H} \parallel \vec{c}$ find a spontaneous net moment of around $0.5 \mu_B$ per formula unit at 2 K. Above T_N^{Dy} , $M(H)$ curves display symmetric magnetization steps at a critical field value that increases with temperature; the size of these steps decreases with increasing temperature, becoming immeasurably small around 40 K.¹⁸ This behavior is remarkably similar to that previously reported in (h) DyMnO_3 ,⁸ but the moment increase associated with the magnetization steps in DYMO is about one half of the increase in (h) DyMnO_3 .

Figure 3(a) displays the intensity of the (1 0 0) magnetic Bragg reflection as a function of field with $\vec{H} \parallel \vec{c}$, measured while increasing the field at temperatures between 4 K and 50 K. For each of these temperatures, we find a sudden drop in the (1 0 0) intensity at a critical field value that increases with temperature. As was shown in Fig. 1 the intensity of the (1 0 0) reflection will be much higher in the intermediate temperature phase than in the low temperature phase, such that this behavior is easily associated with a field induced transition from the intermediate temperature antiferromagnetic phase into the ferrimagnetic phase. The data definitively show a spin reorientation of the Mn moments along with the field induced ferrimagnetic ordering of the Dy moments, as the intensity of this reflection would not drop if the Mn moments remained ordered in the intermediate temperature structure. The intensity of this reflection in the field induced phase is weaker than in zero field at low temperature (the dotted horizontal line represents the expected intensity of the (1 0 0) reflection at 2 K and zero field). This likely arises from a considerably smaller Dy ordered moment, consistent with the smaller magnitude of the magnetization steps at higher temperatures in the $M(H)$ curves. A portion of the H - T phase diagram associated with this transition is shown in Fig. 3(b); it is in perfect agreement with DYMO magnetization data.¹⁸ Interestingly, neutron diffraction is sensitive enough that this transition is still clearly measurable in the 50 K data, while it could not be measured above 40 K in the magnetization data.

The field dependence of the intensities at the (1 0 0) and (3 $\bar{1}$ 0) reflections at $T = 15 \text{ K}$ is displayed in Fig. 4. In panel (a), both reflections show the expected transition at $\mu_0 H_c \approx 1 \text{ T}$; data taken in rising and falling field

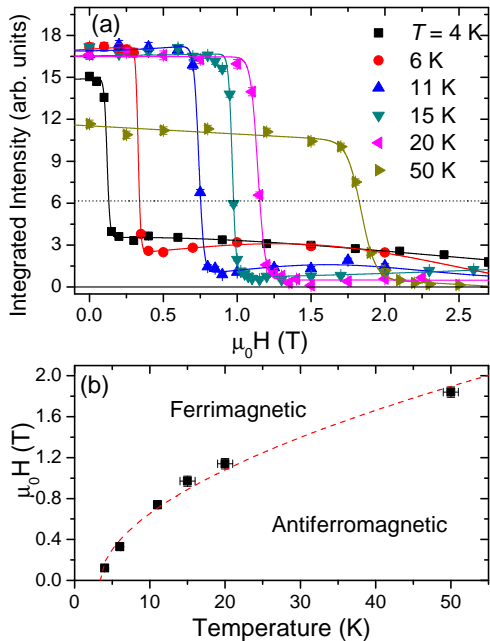


FIG. 3: (color online) (a) Integrated intensity of the (1 0 0) peak as a function field. The data were taken while increasing field. Lines are a guide to the eye. The dotted horizontal line represents the expected intensity at 2 K in zero field. (b) Partial H - T phase diagram showing the transition between the ferrimagnetic and antiferromagnetic phases for $\vec{H} \parallel \vec{c}$.

show only a slight hysteresis, consistent with the small hysteresis of the magnetization steps in the bulk magnetization data. The (3 $\bar{1}$ 0) reflection displays scattering in the low temperature Γ_2 phase and very little scattering in the intermediate temperature phase, such that this change in intensity is likewise consistent with a field induced transition between the two. A more detailed view of the (1 0 0) intensity in the high field region is shown in panel (b). Interestingly, the intensity of this peak rises slowly with increasing field up to about 4 T, but then levels off and actually slightly decreases with increasing field beyond 5 T. This likely reflects the interplay of the ordered moments on the $2a$ and $4b$ Dy sites. The net magnetization of the sample can increase through either an increase of the ordered moment on the $4b$ Dy sites, or through a decrease of the ordered moment (or a reversal of the moment direction) on the $2a$ Dy sites; the former will lead to an increase in the (1 0 0) scattering intensity while the latter will lead to a decrease.

IV. SUMMARY AND CONCLUSIONS

Below $T_N^{\text{Dy}} = 3.4$ K $\text{Dy}_{0.5}\text{Y}_{0.5}\text{MnO}_3$ is magnetically ordered in the Γ_2 irreducible representation with antiferromagnetic Mn order and ferrimagnetic Dy order. Between 3.4 K and 10 K we observe a spin reorientation transi-

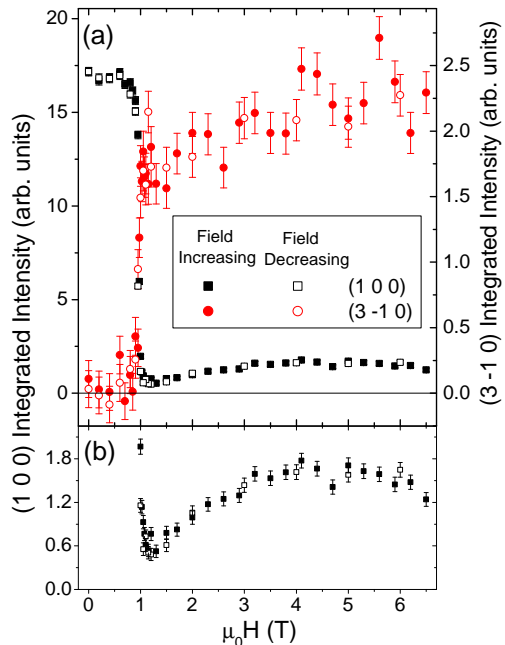


FIG. 4: (color online) (a) Integrated intensities of the (1 0 0) (left scale) and (3 $\bar{1}$ 0) (right scale) peaks measured at $T = 15$ K. Solid symbols represent measurements take while increasing field, open symbols represent decreasing field. (b) Detail of the high field region for the (1 0 0) intensity.

tion of the Mn moments. Antiferromagnetic order of the Mn sites persists up to $T_N^{\text{Mn}} = 70$ K; this magnetic structure of this phase is either Γ_1 or Γ_3 . In this intermediate temperature phase, a magnetic field applied parallel to the c -axis will drive a field induced transition into the low temperature ferrimagnetic phase with relatively little hysteresis.

While hexagonal rare earth manganites have been found to display a variety of magnetic structures, general similarities exist in their phase diagrams. For most (h)RMnO₃ materials featuring a magnetic R^{3+} ion such as $R = \text{Dy, Er, Tm, or Yb}$ the H - T magnetic phase diagram consists of a paramagnetic phase at high temperatures, a Γ_4 antiferromagnetic phase (for the Mn sublattice) at intermediate temperatures, and a Γ_2 ferrimagnetic phase at low temperatures or high magnetic fields^{16,23} ($R = \text{Ho}$ is the important exception to this rule). The Γ_4 and Γ_2 phases are connected through a 90° anti-phase spin reorientation of the Mn moments. (h)RMnO₃ materials with $R = \text{Y, Sc, or Lu}$ display a nonmagnetic rare earth ion, yet still have interesting physics on the Mn sublattice. Optical second harmonic experiments^{1,21,23} have determined that these materials all display a Γ_3 ordering at the lowest temperatures; ScMnO₃ and LuMnO₃ were also reported to feature a Γ_4 phase and an intermediate $P6'_3$ phase. HoMnO₃ is unique, displaying Γ_4 , Γ_3 , and Γ_1 phases.^{11,25} The magnetic phase diagrams of this series can be explored fur-

ther through solid solutions where a nonmagnetic rare earth ion, usually Y, is doped in place of a magnetic ion. Studies of $\text{Ho}_{1-x}\text{Y}_x\text{MnO}_3$ ^{26,27} found that doping with Y increased the temperature range of the Γ_3 phase and partially relieved frustration. In studies of $\text{Er}_{1-x}\text{Y}_x\text{MnO}_3$, Sekhar, *et al.* found evidence for an intermediate state caused by an in phase spin rotation of the Mn moments,²⁴ while Vajk, *et al.* reported that the Γ_4 phase of ErMnO_3 was stable for almost the entire range of doping, $x \leq 0.93$.²⁸

Doping with Y in the case of $\text{Dy}_{0.5}\text{Y}_{0.5}\text{MnO}_3$ has resulted in a unique magnetic phase diagram not previously observed in a hexagonal rare earth manganite. The low temperature phase in DYMO is identical to that observed in (h)RMnO₃ with $R = \text{Dy}, \text{Er}, \text{Tm}, \text{or Yb}$, with the difference being that the magnetic order of the Mn moment in the intermediate temperature phase is Γ_1 or Γ_3 in DYMO rather than Γ_4 . This leads to a qualitatively new magnetic phase diagram. A zero field Γ_1 to Γ_2 spin reorientation transition has not been observed in any other (h)RMnO₃ material; the H - T phase diagram of HoMnO_3 features a boundary between Γ_1 and Γ_2 phases^{20,23,29} at $\mu_0 H \approx 2$ T, yet the transition between them involves multiple distinct intermediate phases.^{11,25} If the intermediate temperature phase is Γ_3 , then the Γ_3 to Γ_2 spin

reorientation transition would involve only half of the Mn ions, in a manner not observed in other (h)RMnO₃ materials. Further experiments on DYMO with complementary techniques such as optical second harmonic spectroscopy and x-ray resonant magnetic scattering will be needed to completely determine the magnetic phases in the intermediate temperature regime, differentiating between the Γ_1 and Γ_3 structures for the Mn sublattice as well as measuring the order of the Dy sublattice. DYMO could prove to be an interesting multiferroic system given the unique magnetic phase diagram and the possibility of strong magnetoelastic coupling near T_N^{Mn} ,¹⁸ and knowledge of the ordered magnetic phases will be needed to fully understand the material.

ACKNOWLEDGEMENTS

We thank J.W. Lynn for guidance and helpful discussions. J.S.H. acknowledges support from the NRC/NIST Postdoctoral Associateship Program. The crystal structures shown in Figure 2 were produced using *VESTA*.³⁰

* email: joel.helton@nist.gov

-
- ¹ D. Fröhlich, St. Leute, V. V. Pavlov, R. V. Pisarev, and K. Kohn, *J. Appl. Phys.* **85**, 4762 (1999).
- ² A. Muñoz, *et al.*, *Phys. Rev. B* **62**, 9498 (2000).
- ³ D. G. Tomuta, S. Ramakrishnan, G. J. Nieuwenhuys, and J. A. Mydosh, *J. Phys.: Condens. Matter* **13**, 4543 (2001).
- ⁴ H. Sugie, N. Iwata, and K. Kohn, *J. Phys. Soc. Jpn.* **71**, 1558 (2002).
- ⁵ A. Muñoz, *et al.*, *Chem. Mater.* **13**, 1497 (2001).
- ⁶ F. Yen, *et al.*, *Phys. Rev. B* **71**, 180407(R) (2005).
- ⁷ O. Prokhnenko, *et al.*, *Phys. Rev. Lett.* **98**, 057206 (2007).
- ⁸ V. Yu. Ivanov, A. A. Mukhin, A. S. Prokhorov, A. M. Balbashov, and L. D. Iskhakova, *Phys. Solid State* **48**, 1726 (2006).
- ⁹ S. Harikrishnan, *et al.*, *J. Phys.: Condens. Matter* **21**, 096002 (2009).
- ¹⁰ B. B. Van Aken, T. T. M. Palstra, A. Filippetti, and N. A. Spaldin, *Nature Mater.* **3**, 164 (2004).
- ¹¹ O. P. Vajk, M. Kenzelmann, J. W. Lynn, S. B. Kim, and S.-W. Cheong, *Phys. Rev. Lett.* **94**, 087601 (2005).
- ¹² T. Lottermoser, *et al.*, *Nature* **430**, 541 (2004).
- ¹³ B. G. Ueland, J. W. Lynn, M. Laver, Y. J. Choi, and S.-W. Cheong, *Phys. Rev. Lett.* **104**, 147204 (2010).
- ¹⁴ S. Lee, *et al.*, *Nature* **451**, 805 (2008).
- ¹⁵ D. P. Kozlenko, S. Kichanov, S. Lee, J.-G. Park, and B. N. Savenko, *J. Phys.: Condens. Matter* **19**, 156228 (2007).
- ¹⁶ C. Wehrenfennig, *et al.*, *Phys. Rev. B* **82**, 100414(R) (2010).
- ¹⁷ S. Nandi, *et al.*, *Phys. Rev. B* **78**, 075118 (2008).
- ¹⁸ Harikrishnan S. Nair, C. M. N. Kumar, H. L. Bhat, Suja Elizabeth, and Th. Bruckel, *Phys. Rev. B* **83**, 104424 (2011).
- ¹⁹ W. Sikora and V. N. Syromyatnikov, *J. Magn. Magn. Mat.* **60**, 199 (1986).
- ²⁰ I. Munawar and S. H. Curnoe, *J. Phys.: Condens. Matter* **18**, 9575 (2006).
- ²¹ M. Fiebig, *et al.*, *Phys. Rev. Lett.* **84**, 5620 (2000).
- ²² S. Nandi, *et al.*, *Phys. Rev. Lett.* **100**, 217201 (2008).
- ²³ M. Fiebig, Th. Lottermoser, and R. V. Pisarev, *J. Appl. Phys.* **93**, 8194 (2003).
- ²⁴ M. C. Sekhar, S. Lee, G. Choi, C. Lee, and J.-G. Park, *Phys. Rev. B* **72**, 014402 (2005).
- ²⁵ O. P. Vajk, M. Kenzelmann, J. W. Lynn, S. B. Kim, and S.-W. Cheong, *J. Appl. Phys.* **99**, 08E301 (2006).
- ²⁶ H. D. Zhou, *et al.*, *Phys. Rev. B* **75**, 132406 (2007).
- ²⁷ R. Vasic, H. D. Zhou, E. Jobiliong, C. R. Wiebe, and J. S. Brooks, *Phys. Rev. B* **75**, 014436 (2007).
- ²⁸ O. P. Vajk, J. Gunasekera, Y. Wang, and T. Heitmann, *J. Appl. Phys.* **109**, 07D910 (2011).
- ²⁹ B. Lorenz, F. Yen, M. M. Gospodinov, and C. W. Chu, *Phys. Rev. B* **71**, 014438 (2005).
- ³⁰ K. Momma and F. Izumi, *J. Appl. Crystallog.* **41**, 653 (2008).